https://doi.org/10.1016/j.tws.2020.107284

A study of net-section resistance of high strength steel bolted connections

Xue-Mei Lin[a,b], Michael C.H. Yam[a,b,*], Kwok-Fai Chung[b,c], and Angus C.C. Lam[d]

[a] *Department of Building and Real Estate, The Hong Kong Polytechnic University, Hong Kong, China*

[b] *Chinese National Engineering Research Centre for Steel Construction (Hong Kong Branch), The Hong Kong Polytechnic University, Hong Kong, China.*

[c] *Department of Civil and Environmental Engineering, The Hong Kong Polytechnic University, Hong Kong, China*

[d] *Department of Civil & Environmental Engineering, University of Macau, Macau, China*

[*] *Corresponding author. E-mail address: michael.yam@polyu.edu.hk*

Abstract

This article presents an experimental and numerical investigation on the net section resistance of high strength steel (HSS) bolted connections subject to double shear. A total of 22 HSS and 11 mild steel (MS) bolted connection specimens were tested to net section fracture. HSS grades of Q690 and Q960, and MS grade of Q345 were studied. Although the HSS material has relatively lower ductility and a lower ratio of tensile strength to yield strength (f_u/f_y) than those of the MS material, in general, the HSS connection specimens were able to reach the connection efficiency (i.e. the ratio of the ultimate load of the connection specimens to the calculated net section resistance) of above 1.0. Subsequently, the structural behaviour of the connections was studied by finite element (FE) analysis. The effects of material ductility and f_u/f_y ratio on the stress development across the net section of the specimens were examined. It was found that HSS materials possess sufficient ductility to allow an efficient stress redistribution across the net section. Besides, the beneficial influence of the 'reinforcement' or the biaxial stress effect due to the presence of holes in the connection increases the ultimate capacity of the perforated

main plate, and hence the HSS specimens were able to reach the net section resistance. However, the overall deformation capability of the HSS specimens was significantly lower than that of the MS specimens. Reliability analysis was carried out to re-examine the partial factor used in the current design equation for predicting the net section resistance in Eurocode 3.

Keywords: High strength steel, Net section resistance, Bolted connections, Experimental investigation, Finite element analysis, Reliability analysis

1. Introduction

High strength steel (HSS) commonly refers to structural steel with nominal yield strength, f_{yn}, higher than 460 MPa [1]. With the development of metallurgical technology, the mechanical properties of HSS have been significantly improved. Steel structures made of HSS can achieve longer span and create larger column-free space with reduced section size and self-weight of the members compared with those made using mild steels (MS) [2-5]. Therefore, considerable economic and environmental benefits can be gained by applying HSS to civil engineering structures. To employ HSS in steel structures effectively, the connections between the HSS structural members, either bolted or welded, must be properly designed to transfer the applied forces. Hence, it is important to ensure an effective stress redistribution across the net section of a bolted connection such that the entire net section can achieve the tensile strength of the material prior to fracture at the bolt hole. To achieve an effective stress redistribution in the connection, the steel material must possess sufficient ductility. However, it is commonly known that HSS generally has relatively lower ductility and a lower ratio of the tensile strength (f_u) to yield strength (f_y) than those of MS materials [6]. It is, therefore, important to examine whether the level of ductility possessed by HSS materials is sufficient for developing an effective stress redistribution across the net section of a HSS bolted connection.

A number of research studies were conducted to investigate the net section resistance ($A_{net}f_u$) of HSS bolted connections, where A_{net} is the net section area of the connection [7-15]. Aalberg and Larsen [9] examined a group of connections equipped with one row of three bolts along the loading direction made of Weldox 460 (f_{yn} = 460 MPa) and Weldox 700E (f_{yn} = 700 MPa). The ultimate loads of the connections were found close to the corresponding net section resistance, $A_{net}f_u$. Može et al. [13] tested several series of single-bolt and two-bolt connections made using S690 steel (f_{yn} = 690 MPa). It was found that the design equation for ultimate resistance of net section in EN 1993-1-1 [16], i.e. Eq.(1), provided conservative prediction for HSS sections.

$$N_{u,Rd} = \frac{0.9A_{net}f_u}{\gamma_{M2}} \tag{1}$$

where γ_{M2} with a recommended value of 1.25 is the partial factor for the resistance of cross-section in tension to fracture [16]. This finding was further confirmed by Feldmann et al. [12] based on a study of single bolted connections made of S960 steel (f_{yn} = 960 MPa). It was even suggested that the steel grade range (S460 ~ S700) in EN 1993-1-12 could be extended to include S960 [12]. However, the conclusions above were mainly developed based on the study of multi-bolt connections but steel grade only up to S690/S700, or single-bolt connections with steel grade up to S960. Therefore, the applicability of these findings to multi-bolt connections made of HSS up to S960 needs further investigation. A preliminarily numerical study has been carried out by the authors to examine the ultimate strength of multi-bolt connections made of S960 steel [17]. It was found that the ultimate strength of the multi-bolt HSS connections could reach the corresponding net section resistance. Although the above studies showed that the HSS connections with single or two bolts in the net section were able to reach the corresponding net section resistance, there is limited experimental data on the study of ultimate strength of multi-bolt connections made of HSS, especially for steel grade up to S960. Hence, this study aims to examine experimentally the ultimate strength of multi-bolt connections made of various HSS materials (grade Q690 and Q960) and with different connection details. A numerical study using the finite element (FE) method is also conducted to help explain the test results and to provide further insights. Finally, a reliability analysis is conducted to assess the partial factors in the current design formula in Eurocode 3 [16, 18] for evaluating the net section strength of HSS connections based on the test data from this paper and those extracted from the existing literature.

2. Experimental investigation

2.1 Test specimens

A total of 22 HSS and 11 MS bolted butt connection specimens subject to double shear were tested. A 2 × 2 bolt pattern was adopted for the specimens with four Grade 12.9 M12 bolts as shown in Fig. 1. The geometric parameters included the edge distance (e_2), end distance (e_1), bolt spacing parallel and perpendicular to the loading direction (p_1 and p_2), and the bolt hole diameter (d_0), as presented in Fig. 1. Three types of steel grade, namely, Q345, Q690 and Q960, were investigated in this study, as represented by letters M1, M2 and M3, respectively in the specimen designation. The nominal main plate thickness (t) was 6 mm for the Q345 and Q690 steel plates, and 5 mm for the Q960 steel plate. All the lap plates were made using 10 mm thick Q690 steel plate to ensure the occurrence of fracture in the main plate. The edge distance (e_2) ranged from $0.8d_0$ to $2.0d_0$, i.e. from 10 to 26 mm with the bolt hole diameter (d_0) of 13 mm. The bolt spacing perpendicular to the loading direction (p_2) varied from $2.0d_0$ to $4.4d_0$ (i.e. from 26 to 57 mm). The bolt spacing in the direction of load transfer (p_1) and the end distance (e_1) was both maintained at $3.0d_0$ (i.e. 39 mm) to avoid block shear failure and bearing failure. The specimens were designated using steel grade, edge distance (e_2), and bolt spacing p_2. For example, considering specimen M1e26p39, 'M1' represents the steel grade Q345, 'e26' represents the edge distance e_2 = 26 mm, and 'p39' represents the bolt spacing perpendicular to the loading direction p_2 = 39 mm. The measured dimensions are summarised in Table 1.

Tension coupon tests were conducted according to ASTM E8/E8M-16a standard (ASTM 2016) [19]. Three dog-bone shaped tension coupons were tested for each type of steel material. The mean values of the measured material properties, including elastic modulus (E), static yield strength (f_y), static tensile strength (f_u), ultimate strain (ε_u) based on 50 mm gauge length and elongation at fracture (Δ), are summarised in Table 2. Typical stress-strain curves of the MS and HSS material are depicted in Fig. 2. It is noted that the measured static yield strength of steel grade Q960 is 930.2 MPa, slightly lower than the nominal yield strength of 960 MPa.

2.2 Test setup and procedure

All the tests were carried out using a universal tensile testing machine (INSTRON 8803) with a loading capacity of 500 kN. The test setup is shown in Fig. 3. The ends of the connection specimen were fixed in the corresponding hydraulic grip. A quasi-static tensile load was applied to the specimen by the bottom grip. The built-in load cell and displacement transducer recorded the applied load level and the total elongation of the specimen, respectively. In addition, two linear variable differential transformers (LVDTs) were installed on both sides of the main plate to measure the relative displacement between two points of 125 mm apart, as shown in Fig. 3. The reading of the LVDTs was collected by a data logger system (UCAM-60B). The bolts were snug tightened by hand to minimise any frictional resistance of the connection.

Each specimen was subject to a preloaded of 10 kN to eliminate any major slip between the bolts and bolt holes. The preload was then released to around 2 kN to ensure the majority of the bolts bearing on the bolt-hole walls. The main loading procedure comprised of two stages: a load control at 20 kN interval in the elastic stage followed by a stroke control in the inelastic stage. The displacement loading rate was specified to be 0.5 mm and 0.3 mm per minute for the MS and HSS connections, respectively, until reaching the corresponding ultimate load. Subsequently, the loading rate was increased to 1.0 mm and 0.5 mm per minute, respectively, until the failure of specimens. At the end of each loading step, the stroke was held for around 2 minutes to allow for stress redistribution and the corresponding static readings of load were recorded.

2.3 Test results

All the 33 specimens were failed by net section fracture of the main plate. The failure mode of the specimens is shown in Fig. 4. As expected, fracture occurred in the main plate at the first row of bolts. The ultimate load from the tests, $P_{u,test}$, the calculated net section resistance P_{us}, i.e. $A_{\mathrm{net}}f_{\mathrm{u}}$, and the connection efficiency of each connection, which is the ratio of $P_{u,test}$ to P_{us}, are summarised in Table 1. In general, the test results showed that the connection specimens could reach the corresponding net section resistance. The average connection efficiency was 1.11 with a coefficient of variation (CoV) of 3.8% and 1.09 with a CoV of 3.0% for the MS and HSS specimens, respectively.

The load-displacement curves for all the specimens are shown in Fig. 5, where the value of displacement was determined by the mean value of the two LVDTs readings. The load-displacement curve of specimen M2e10p26 after the ultimate state was not shown due to unexpected termination by the testing machine. The corresponding structural performance after the ultimate state has been duplicated using numerical simulation which will be discussed in the later section. In general, a linear load-displacement response was found at the initial stage for all the curves and then followed by a nonlinear load-displacement response once the yielding of material occurred. For the MS specimens, obvious load plateaus were observed, resulting in a larger deformation of the MS specimens when comparing to those of the HSS connection specimens. This observation is expected since the higher ductility of the MS material allowed an effective stress redistribution in the vicinity of the bolt holes, which permitted further elongation to occur along the length of the specimen prior to the fracture of the net section. On the other hand, the load-deformation curves of HSS specimens did not possess an appreciable yield plateau. The ultimate load was achieved rapidly after yielding of the critical net section, followed by necking and fracture of the whole net section, due to the low f_u/f_y ratio of the HSS materials as shown in Fig. 5.

2.4 Discussion of test results

As shown in Table 1, the ultimate load of the specimens increased significantly with increasing edge distance (e_2) from 10 to 26 mm for a bolt spacing (p_2) of 26 or 39 mm irrespective of steel grade. It was because the net section area of the steel plate (A_{net}) increases with increasing edge distance (e_2), as shown in Table 1. However, the corresponding connection efficiency decreased with increasing edge distance (e_2). As shown in Fig. 6a, for Q345, Q690 and Q960 specimens with a bolt spacing (p_2) of 26 mm, i.e. specimens (M1-M3)(e10-e26)p26, the connection efficiency decreased from 1.21 to 1.06, from 1.16 to 1.04, and from 1.12 to 1.03, respectively, with increasing edge distance from 10 to 26 mm. A similar decreasing tendency was also observed among the specimens with a bolt spacing (p_2) of 39 mm, i.e. specimens (M1-M3)(e10-e26)p39, although the reduction is not very severe, as shown in Fig. 6b. This may be due to the insufficient stress redistribution along a longer edge distance prior to failure. Further clarification will be presented in the later section of the finite element analysis of test specimens. In addition, for specimens (M1-M3)e10p57, (M1-M3)e20p39 and (M1-M3)e26p26, the width (W) was maintained at $6.0d_0$, which means that the designed net section capacity was maintained the same for each specimen series made using the same steel material. The edge distance was varied from 10 to 26 mm, and the corresponding bolt spacing (p_2) was decreased from 57 to 26 mm. As shown in Fig. 6c, the connection efficiency also decreased in general with increasing edge distance (e_2) for each steel grade. Moreover, as shown in Fig. 6d, the connection efficiency of specimens with an edge distance (e_2) of 20 mm was found all below that of the specimens with an edge distance (e_2) of 10 mm.

For the effect of bolt spacing (p_2), the ultimate load of the specimens with an edge distance (e_2) of 10 or 20 mm also increased with increasing bolt spacing (p_2) from 26 to 57 mm or 52 mm irrespective of the steel grade, as shown in Table 1. This was also due to the increasing net section area of the steel plate (A_{net}) with the increase in the bolt spacing (p_2). However, the connection efficiency decreased with increasing bolt spacing (p_2) for the specimens (M1-M3)e10(p26-p57), as shown in Fig. 6d. Again, this may be attributed to the insufficient stress redistribution along a longer bolt spacing (p_2) before failure due to the stress concentration at the inside edge of the bolt hole. For the specimens with a longer edge distance ((M1-M3)e20(p26-p52)), the connection efficiency increased with the increase in p_2 from 26 to 39 mm in general, as shown in Fig. 6d. This may be due to the fact that the stresses could be further redistributed along the longer edge distance (20 mm) prior to the fracture of the inside edges of the bolt holes when the bolt spacing (p_2) was increased from 26 to 39 mm. Hence, the connection efficiency was higher for a larger bolt spacing (p_2). However, the connection efficiency was not found to increase when the bolt spacing (p_2) was further increased up to 42 mm.

As shown in Fig. 7a, a slight decline trend in the connection efficiency was found with increasing yield strength of steel material for the specimens with the same geometric configuration. The maximum difference of the connection efficiency was found between specimens M1e10p26 and M3e10p26, with a value of 7.7%. However, the connection efficiencies of all the HSS specimens are above 1.0. This could imply that the lower ductility and f_u/f_y ratio might not significantly affect the net section resistance of the HSS connections. It may be attributed to two reasons: firstly, although the HSS material has lower ductility than that of the MS material, the HSS materials possess sufficient ductility to allow an effective stress redistribution around the bolt holes; secondly, the net section strength was enhanced by the biaxial stress effect in the perforated steel plate [20-22]. This will be further illustrated in the later section of the finite element analysis of test specimens. However, the influence of lower ductility of steel material on the specimen deformation was obvious, as shown in Fig. 7b. The specimens with the same geometric configurations made with the higher-grade steel material generally showed a smaller axial displacement, which was measured by the LVDTs at the peak load. This could also be observed in the corresponding load-displacement curves shown in Fig. 5.

3. Numerical investigation

3.1 Finite element model

The finite element (FE) method was employed to simulate the structural behaviour of the specimens. The development of stress and strain along the critical net section and the deformation of the bolt holes during the loading, which could not be observed during the tests due to the configuration of lap plates, would be examined carefully using the FE analysis results. The FE results would also help explain the test results, in particular, the reason behind the attainment of the net section resistance of the HSS specimens.

Nonlinear FE analysis of the connection specimens was conducted using the commercial software, ABAQUS/Explicit [23]. The C3D8R solid elements were used to model all the connected components, including the main plate, lap plate and bolt, as shown in Fig. 8. The head of the bolt was modelled by a cylinder with a diameter of 20 mm. A mesh convergence study was performed to determine the suitable mesh size with reasonable simulation accuracy and computation time. A refined mesh size of 1.5 mm was used in the vicinity of the bolt holes in the main plate. The mesh sizes for the lap plate and the bolt were approximately 4 mm and 2 mm, respectively. The interactions between the surfaces of contact were defined as general contact with "hard" contact behaviour. A friction coefficient of 0.2, which was specified as the Class D slip factor for the untreated hot rolled steel in EN 1993-1-8 [24] was adopted for the tangential contact behaviour. A fixed boundary was applied to one end of specimens to simulate the fixed end of the connection. A quasi-static uniform displacement along the longitudinal direction (U1) was applied on the other end of the specimens to simulate the applied load in the test, and the remaining five degrees of freedom were restrained, as shown in Fig. 8. Besides, the shanks of bolts were set into bearing on the surfaces of the bolt holes in the initial stage to simulate the results of the preload step in the test.

The elastic-plastic material behaviour with isotropic hardening was adopted for the analysis. The true stress-strain relationship before necking was determined by Eqs. (2) and (3) based on the values of engineering stress and strain obtained from the tension coupon tests. The corresponding relationship after necking was considered almost linear according to [25] and was calibrated by the modified weighted average method proposed by Jia and Kuwamura

[26]. The material properties of the Grade 12.9 M12 bolts were selected from [27]. The elastic modulus, yield strength, ultimate strength and the ultimate strain were taken as 211.1 GPa, 1210 MPa, 1310 MPa, and 3.25%, respectively.

$$\sigma_{true} = \sigma_{eng}\left(1 + \varepsilon_{eng}\right) \tag{2}$$

$$\varepsilon_{true} = \ln\left(1 + \varepsilon_{eng}\right) \tag{3}$$

where σ_{true} and ε_{true} are true stress and strain, σ_{eng} and $\varepsilon_{\mathrm{eng}}$ are engineering stress and strain, respectively. The material model was used in conjunction with the simplified Johnson-Cook fracture model (Eq. (4)) in order to capture the structural behaviour at fracture of the specimens [28-30]. When the parameter *D*, as presented in Eq. (5), reached 1.0, the material stiffness was considered to be fully degraded [31], and the related elements were removed from the calculations to simulate the fracture.

$$\bar{\varepsilon}_f^{pl} = C_1 + C_2 e^{-C_3 \eta} \tag{4}$$

$$dD = \frac{L}{\bar{u}_f^{pl}} d\left(\bar{\varepsilon}^{pl}\right) \tag{5}$$

where $\bar{\varepsilon}_f^{pl}$ is the equivalent plastic strain to fracture, η is the stress triaxiality, which equals to the ratio of the mean normal stress (σ_m) to the von Mises equivalent stress ($\bar{\sigma}$) [29, 32]. *L* is the characteristic length of the element and $\bar{u}_f^{pl}$ is the effective plastic displacement at the point of failure. The values of *L* vary with different element geometries and are automatically calculated by ABAQUS [23]. Due to the lack of experimental data, a value of 0.1 was assigned to $\bar{u}_f^{pl}$ with a linear evolution form for each steel material [33]. C_1, C_2 and C_3 are material parameters, which were calibrated using a trial and error process until the gradual unloading responses predicted by the FE analysis were in good agreement with those in the test [34, 35]. Based on the above, the parameters C_1 and C_2 were determined as 0.08 and 2.0 for the three steel grades. The parameter C_3 was calibrated to be 3.2, 2.5 and 2.8 for Q345, Q690 and Q960 steel material, respectively.

3.2 **Results of finite element analysis and discussion**

The predicted failure mode of the specimens by the FE analysis compared well with the observed net-section fracture of the specimens in the tests as shown in Fig. 4. The ratio of the ultimate load between test results and the predictions from FE analysis, i.e. $P_{u,test}/P_{u,FEM}$ is summarised in Table 1. The test-to-predicted ratio for the Q345 specimens varied from 0.98 to 1.05 with an average value of 1.01 and a CoV of 2.0%. For the HSS specimens, the test-to-predicted ratio ranged from 0.98 to 1.04 with an average of 1.01 and a CoV of 1.4%, as shown in Table 1. In general, the FE load-displacement curves of all the specimens were in good agreement with those from the test results as illustrated in Fig. 5. It can be seen that the FE analysis was able to capture the nonlinear behaviour of all the specimens as well as the descending branch of the load-displacement curves.

The FE models of specimens (M1-M3)e20p39 were used to illustrate the typical deformation process of the connections. Three stages of loading as shown in the corresponding loading-displacement curves in Fig. 5 were considered, i.e. $P_1 = 0.6P_{u,FEM}$, $P_2 = 0.9P_{u,FEM}$, and $P_3 = 1.0P_{u,FEM}$. The corresponding development of the axial stress (S_{11} – along the loading direction) and the equivalent plastic strain (PEEQ) across the critical net section are illustrated in Fig. 9. The value of stress S_{11} was compared with the average normal stress across the critical net section at the corresponding loading stage, i.e. P_i / A_{net}, i = 1, 2 and 3, as well as the yield and tensile strength of the corresponding material. The critical net section is shown in Fig. 8a as segment A_1-B_1-C_1-C_2-B_2-A_2.

As shown in Fig. 5, the three specimens maintained nearly linear load-displacement behaviour before the load reaching $0.6P_{u,FEM}$, and thus the value of PEEQ along the A_1-B_1-C_1-C_2-B_2-A_2 at $0.6P_{u,FEM}$ state was found nearly zero, as illustrated in Fig. 9. When the load was increased to $0.9P_{u,FEM}$, large values of PEEQ at the bolt edges, i.e. at points B_1, C_1, B_2 and C_2 in specimen M1e20p39 were observed, which was due to the much larger deformation around the bolt hole edges than that in other areas across the net section at the $0.9P_{u,FEM}$ state. At the $1.0P_{u,FEM}$ loading stage, the PEEQ around the bolt holes became more significant as shown in Fig. 9a. For specimens M2e20p39 and M3e20p39, the PEEQ in the vicinity of the bolt holes was relatively small at the $0.6P_{u,FEM}$ state. At the ultimate state, the PEEQ increased substantially around the bolt holes as illustrated in Figs. 9b and 9c for the HSS specimens. However, the corresponding values of PEEQ around the bolt holes were lower than those in the MS specimens at the ultimate state due to the lower ductility of HSS materials.

The distribution of stress S_{11} across the critical net section was highly non-uniform at the $0.6P_{u,FEM}$ loading stage for the three specimens due to the stress concentration around the bolt holes, as shown in Fig. 9. When the load was increased to $0.9P_{u,FEM}$, stress redistribution occurred in the plate areas between the two bole holes, i.e. along segment C_1-C_2, as shown in Fig. 9. The average normal stresses S_{11} across the critical net section, i.e. P_2/A_{net} for the three specimens were all found exceeding the corresponding yield strength level of the steel materials and even already approaching the tensile strength level at this stage for the three specimens. For specimen M1e20p39, the whole critical net section has completely yielded at $0.9P_{u,FEM}$ loading stage. While for specimens M2e20p39 and M3e20p39, the stresses along segments A_1-B_1 and A_2-B_2 (i.e. the edge distance) were not fully developed up to the yield strength at this loading stage, especially those in the vicinity of the plate edge, as shown in Figs. 9b and 9c. This was consistent with the observation that the corresponding values of PEEQ close to the edges of the plate were nearly zero at the $0.9P_{u,FEM}$ loading stage. When the load reached $1.0P_{u,FEM}$, the stress along segment C_1-C_2 was further developed and exceeded the stresses at the inside edge of the bolt holes for the three specimens. This observation is due to the biaxial stress state existing in the plate area away from the bolt holes. Further discussion of the beneficial effects of biaxial stress state will be discussed in the following section. The resulting mean normal stress across the critical net section at the ultimate state, i.e. P_3/A_{net}, was far above the tensile strength level of the corresponding material although the local stress S_{11} nearby the plate edges, i.e. A_1 and A_2, was still relatively lower than the tensile strength level. Hence, it can be seen that the net section resistance could be achieved for the multi-bolt HSS connections even though the HSS materials have lower ductility and lower f_u/f_y ratio than those of MS materials.

Based on the analysis above, it was found that both MS and HSS materials provided sufficient ductility to allow efficient stress re-distribution across the net section of the specimens and avoided the occurrence of premature fracture at the bolt holes. However, the stresses were always non-uniformly distributed along the segments A_1-B_1 and A_2-B_2 throughout the whole loading process and the stresses at the plate edge were always below the corresponding tensile strength of the material. The major contribution to the net section resistance of the connection was mainly from the highly stressed area between the bolt holes (C_1-C_2) and the area near the outside edge of the bolt holes (B_1 and B_2). This may be explained by the beneficial influence of the 'reinforcement' or the biaxial stress effect caused by the two bole holes, which was first proposed by Munse and Chesson [21] based on the study conducted by Schutz [20]. It had been found that the biaxial stress effect could enhance the ultimate strength of a perforated steel plate at the net section [22]. The stress vectors of specimen M3e20p39 at the $0.9P_{u,FEM}$ loading stage is shown in Fig. 10 to illustrate the biaxial stress effect. As shown in the figure, tensile stresses along the transverse direction, i.e. S_{22} were observed across the critical net section. The value of S_{22} could further increase with increasing applied tensile load. It can be seen that S_{22} was nearly zero across the gross section (D_1-D_2) located far from the bolt holes in the main plates, as shown in Fig. 10. The biaxial state of stress is due to the existence of bolt holes that prevented the free lateral contraction of the material in the net section area when the specimen is subject to tension [36]. It was proposed that the failure of most ductile materials could be accurately predicted by the distortion energy criterion, i.e. $(\sigma_1 - \sigma_2)^2 + (\sigma_2 - \sigma_3)^2 + (\sigma_1 - \sigma_3)^2 = 2{\sigma_v}^2$, where σ_1, σ_2 and σ_3 are the principal stresses and σ_v is the equivalent von Mises stress [37]. Due to the biaxial state of stress (σ_1 = S_{11}, σ_2 = S_{22} and σ_3 = 0), a larger value of S_{11} is required in order for the material to reach the corresponding tensile strength compared with the same material under uniaxial tension [37]. As shown in Fig. 10, S_{22} in the area between the bolt holes (C_1-C_2) and the area near the outside edge of the bolt holes (B_1 and B_2) was much larger than those in other regions across the net section. This resulted in a larger enhancement of S_{11} in the corresponding areas than those in other areas, and the consequent value of S_{11} exceeded that around the bolt holes at the ultimate state, as shown in Fig. 9.

4. Reliability analysis and design recommendations

The net section resistance of HSS (S460~S700) based on the EN 1993-1-12 [18] addition rule is:

$$N_{t,Rd} = \frac{0.9 A_{net} f_u}{\gamma_{M12}} \tag{6}$$

where γ_{M12} is the partial factor for net section resistance of HSS (S460~S700) with a value of 1.25 [18]. It is worth noting that Eq. (1) was mainly developed based on the test data of MS bolted connections [38]. The factor 0.9 in Eq. (1) was initially suggested for MS bolted connections to meet the reliability criteria and maintain the specified value of 1.25 for partial factor γ_{M2} which was also employed in other design standards, such as EN 1993-1-8 [24] to predict the resistance of bolted connections in tension [16, 39]. Since Eq. (6) is only applicable to steel grade up to S700, a reliability analysis of the bolted connections with higher steel grade

(Q960) should be conducted. In addition, the new HSS connection data from this study would also help substantiate the application of Eq. (6) to HSS connections.

According to EN 1990 [40], the target value of reliability index β was taken as 3.8 corresponding to a structure under the ultimate limit state for a 50-year reference period. The first-order reliability method (FORM) sensitivity factor for resistance α_R was taken as 0.8 to obtain a product of $\alpha_R\beta = 0.8 \times 3.8 = 3.04$ corresponding to a probability of failure of about 0.1%. A partial factor γ_M, which accounts for material properties, model uncertainties, and dimensional variations, equals to the ratio between the characteristic and the design values of resistance, presented as [40]

$$\gamma_M = \frac{r_k}{r_d} \tag{7}$$

$$r_k = b g_{rt}\left(\underline{X}_m\right) R_k \tag{8}$$

$$r_d = b g_{rt}\left(\underline{X}_m\right) R_d \tag{9}$$

$$R_k = \exp(-k_\infty \alpha_{rt} Q_{rt} - k_n \alpha_\delta Q_\delta - 0.5Q^2) \tag{10}$$

$$R_d = \exp\left(-k_{d,\infty} \alpha_{rt} Q_{rt} - k_{d,n} \alpha_\delta Q_\delta - 0.5Q^2\right) \tag{11}$$

If the number of tests *n* is larger than 100, the values of R_k and R_d can be obtained by

$$R_k = \exp(-k_\infty Q - 0.5Q^2) \tag{12}$$

$$R_k = \exp(-k_\infty Q - 0.5Q^2) \tag{13}$$

where *b* is the mean value correction factor, which can be estimated by 'least squares' best-fit method, presented as

$$b = \frac{\sum r_e r_t}{\sum {r_t}^2} \tag{14}$$

where r_e and r_t are experimental and theoretical values of resistance. $g_{rt}(\underline{X})$ is a design model for theoretical resistance, which equals to $A_{net}f_u$ in this study. Value of $g_{rt}\left(\underline{X}_m\right)$ was determined by the mean value of the nominal net section area and the mean value of measured tensile strength of steel material. k_n and $k_{d,n}$ are the characteristic and design fractile factors. The corresponding values were determined according to [41, 42] based on the number of tests n. k_∞ and $k_{d,\infty}$ are the values of k_n and $k_{d,n}$ for infinite n, taken as $k_\infty = 1.64$ and $k_{d,\infty} = \alpha_R \beta = 3.04$ [40]. Parameters, including Q_{rt}, Q_δ and Q can be determined by the coefficients of variation V_r, V_δ and V_{rt}, based on the expressions of $\sqrt{\ln({V_{rt}}^2+1)}$, $\sqrt{\ln({V_\delta}^2+1)}$, and $\sqrt{\ln({V_r}^2+1)}$, respectively. α_{rt} and α_δ are the weighting factor, equals to Q_{rt}/Q ratio and Q_δ/Q ratio, respectively. V_δ is the coefficient of variation of the error terms δ, which is combined with the coefficients of variation of other basic variables in the design model, i.e. V_{Xi}. The coefficient of variation (CoV) value of the material property was taken as 0.055 for HSS material according to [43]. The CoV values of the hole diameter, plate width and plate thickness were taken as 0.005, 0.005 and 0.05, respectively according to [44, 45]. The relationship among these coefficients of variation is given by

$$ {V_r}^2 = {V_\delta}^2 + {V_{rt}}^2 \tag{15} $$

$$ {V_{rt}}^2 = \sum_{i=1}^{j} {V_{Xi}}^2 \tag{16} $$

where j is the number of different variations. More detailed procedure of determining the various parameters can be found in [40, 46]. In addition, another basic variable contained in the design model, which is defined as a nominal value should be considered. For example, the mean values of the geometric dimensions are adopted as the nominal values, and the nominal values of the material properties are defined as characteristic values. The characteristic value of the material strength can be obtained based on previous knowledge. Thus, the nominal resistance r_n can be calculated using the mean value of the nominal net section area and characteristic value of measured tensile strength of steel material. In this study, it can be presented as

$$r_n = g_{rt}(\underline{X}_n) = g_{rt}(\underline{X}_m)exp(-2.0V_r - 0.5V_r^{\ 2}) \tag{17}$$

where the value of V_r should be taken as the maximum variation coefficient obtained from prior tests. Subsequently, the discrepancy between the characteristic and the nominal value of resistance should be considered to modify the partial factor γ_M. The ratio between the characteristic and the nominal value of resistance is presented as

$$k_c = \frac{r_n}{r_k} \tag{18}$$

Finally, the corrected partial factor $\gamma_M{}^*$ via using nominal resistance is obtained by

$$\gamma_M{}^* = k_c\gamma_M \tag{19}$$

The results of the statistical analysis of the new HSS connection data from this study, defined as set 1, are summarised in Table 3. The value of the corrected partial factor $\gamma_M{}^*$ for set 1 is found to be 1.066 based on the analysis of the design model $A_{net}f_u$, The corresponding value of $\gamma_M{}^*$ could even be declined to 0.960 if the factor of 0.9 was considered in the design model ($0.9A_{net}f_u$). This implies that the current design equation in EN 1993-1-12 provides conservative predictions of the net section resistance of HSS bolted connections, which is also consistent with the findings from [12, 13] and [47]. To ensure the sample could sufficiently reflect the probabilistic distribution of the population in statistical evaluation, a large number of test results are needed [40]. Therefore, a total of 137 test results of HSS bolted connections failed by net section fracture were also evaluated, including the 22 connections tests in this study and 115 specimens made using HSS selected from existing literature [8, 9, 11-14, 48], as shown in Fig. 12. The number of bolts in the net section (N_b) ranges from one to three. The width and thickness of the main plate (W and t) range from 41 to 242 mm and 5.0 to 17.5 mm, respectively. The bolt diameter (d_0) varies from 13 to 32 mm. The measured yield strength and tensile strength (f_y and f_u) vary from 460 to 1060 MPa and from 556 to 1161 MPa, respectively, as shown in Table 4. The 137 test results, defined as set 2, were divided into two sub-sets (set 3 and set 4) according to the measured values of yield strength of steel material. The specimens made using steel material with yield strength lower than 700 MPa were included in Set 3, the remaining were contained in Set 4. The statistical evaluation of each set of data was carried out and the corresponding results are summarized in Table 3. The value of the corrected partial factor $\gamma_M{}^*$ for set 2, 3 and 4 are found to be 1.118, 1.080 and 1.170, respectively based on the analysis of the design model $A_{net}f_u$. The value of $\gamma_M{}^*$ could be declined to 1.006, 0.972 and 1.053 for Set 2, 3 and 4, respectively for the design model $0.9A_{net}f_u$. It can be seen that the set 4 data, which contains test specimens with a yield strength greater than 700 MPa, has the largest $\gamma_M{}^*$, which reflects the larger variation of net section resistance of this type of specimen. This is also consistent with the observation that the CoV values of $V_\delta = 0.049$, and $V_r = 0.089$ in set 4 data are largest among the three sets. Again, this indicates that the predicted net section resistance of HSS bolted connections by the current design formula in EN 1993-1-12 is very conservative.

5. Summary and conclusions

An experimental and numerical investigation on the net section resistance of multi-bolt HSS connection specimens is presented in this study. A total of 22 high strength steel and 11 mild steel bolted connections were tested to failure by net section fracture. The test results showed that the connection efficiencies of all the specimens were larger than 1.0, which indicated that the multi-bolt HSS connections could achieve the corresponding net section resistance ($A_{net}f_u$).

Finite element analysis was conducted to simulate the structural behaviour of the specimens in order to further examine the nonlinear stress and strain development at the critical net section. The analysis also helped investigate the effects of material ductility and f_u/f_y ratio on the structural performance of the connection specimens. It was found that the relatively lower ductility and lower f_u/f_y ratio of HSS materials than those of MS materials did not affect the net section resistance of HSS connections significantly. The attainment of the net section resistance of the multi-bolt HSS connections was mainly due to two reasons: (1) the lower ductility of the HSS materials was still sufficient to allow an efficient stress redistribution across the net section, and (2) the ultimate capacity of the perforated main plate was enhanced due to the biaxial stress effect caused by the bole holes. However, the overall deformation capability of the HSS specimens was significantly lower than that of the MS specimens due to the low ductility of HSS materials.

In addition, the partial factor in the current design equation was re-examined by a statistical evaluation of the 22 new HSS connection data from this study. The value of the corrected partial factor $\gamma_M{}^*$ was found to be 1.066 based on the analysis of the design model $A_{net}f_u$, The corresponding value of $\gamma_M{}^*$ could be declined to 0.960 if the factor of 0.9 was considered in the design model ($0.9A_{net}f_u$). Furthermore, a statistical analysis of a larger sample size (137 test data) including 115 test data extracted from existing literature and 22 from current study was also carried out. The value of the corrected partial factor $\gamma_M{}^*$ was found to be 1.118 and 1.006 for the design models $A_{net}f_u$ and $0.9A_{net}f_u$, respectively. It implied that the current design equation for net section resistance of HSS (S460~S700) in EN 1993-1-12 with a partial factor of 1.25 provided conservative predictions of the HSS bolted connection specimens.

Acknowledgements

The work described in this paper is fully supported by a grant from the Chinese National Engineering Research Centre (CNERC) for Steel Construction (Hong Kong Branch) at The Hong Kong Polytechnic University (Project No. 1-BBYQ). The constructive comments from Dr Tak-Ming Chan and Dr Junbo Chen for improving the reliability analysis discussion are highly appreciated. The technical assistance during the experimental investigation provided by Mr C.F. WONG, Mr M.C. Ng and Mr Y.H. Yiu is also gratefully acknowledged.

References

[1] G. Shi, F.X. Hu, Y.J. Shi, Recent research advances of high strength steel structures and codification of design specification in China, International Journal of Steel Structures. 14(4). (2014). 873-887. https://doi.org/10.1007/s13296-014-1218-7.

[2] H.-P. Günther, Use and application of high-performance steels for steel structures, IABSE-AIPC-IVBH, Switzerlandr, 2005.

[3] R. Bjorhovde, Performance and Design Issues for High Strength Steel in Structures, Advances in Structural Engineering. 13(3). (2010). 403-411. https://doi.org/10.1260/1369-4332.13.3.403.

[4] G. Shi, X. Zhu, H.Y. Ban, Material properties and partial factors for resistance of high-strength steels in China, Journal of Constructional Steel Research. 121. (2016). 65-79. https://doi.org/10.1016/j.jcsr.2016.01.012.

[5] C.K. Lee, S.P. Chiew, J. Jiang, Residual stress study of welded high strength steel thin-walled plate-to-plate joints, Part 1: Experimental study, Thin-Walled Structures. 56. (2012). 103-112. https://doi.org/10.1016/j.tws.2012.03.015.

[6] Y. Fukumoto, New constructional steels and structural stability, Engineering structures. 18(10). (1996). 786-791. https://doi.org/10.1016/0141-0296(96)00008-9.

[7] P. Može, Ductility and resistance of bolted connections in structures made of high strength steels, Politehnica University of Timisoara, Romunija, 2008.

[8] Y.B. Wang, Y.F. Lyu, G.Q. Li, J.Y.R. Liew, Behavior of single bolt bearing on high strength steel plate, Journal of Constructional Steel Research. 137. (2017). 19-30. https://doi.org/10.1016/j.jcsr.2017.06.001.

[9] A. Aalberg, P. Larsen, Strength and ductility of bolted connections in normal and high strength steels, 1999.

[10] A. Aalberg, P. Larsen, Strength and ductility of bolted connections in normal and high strength steels, Proceedings of the seventh international symposium on structural failure and plasticity, 2000.

[11] R. Puthli, O. Fleischer, Investigations on bolted connections for high strength steel members, Journal of Constructional Steel Research. 57(3). (2001). 313-326. https://doi.org/10.1016/s0143-974x(00)00017-1.

[12] M. Feldmann, N. Schillo, S. Schaffrath, K. Virdi, Rules on high strength steel (RUOSTE), Luxembourg. 2016. https://doi.org/10.2777/908095.

[13] P. Može, D. Beg, J. Lopatič, Net cross-section design resistance and local ductility of elements made of high strength steel, Journal of Constructional Steel Research. 63(11). (2007). 1431-1441. https://doi.org/10.1016/j.jcsr.2007.01.009.

[14] K. Udagawa, T. Yamada, Failure modes and ultimate tensile strength of steel plates jointed with high-strength bolts, Journal of Structural and Construction Engineering, Architectural Institute of Japan. 505. (1998). 115-22.

[15] M.C.H. Yam, K. Ke, B. Jiang, A.C.C. Lam, Net section resistance of bolted S690 steel angles subjected to tension, Thin-Walled Structures. 151. (2020). 106722. https://doi.org/10.1016/j.tws.2020.106722.

[16] European Committee for Standardization (CEN), BS EN 1993-1-1: Eurocode 3: Design of steel structures-Part 1-1: General rules and rules for buildings, 2005.

[17] X.-M. Lin, M.C.H. Yam, K.-F. Chung, A.C.C. Lam, Numerical investigation into net-section resistances of high strength steel bolted connections, International Conference on Engineering Research and Practice for Steel Construction 2018. (2018).

[18] European Committee for Standardization (CEN), BS EN 1993-1-12: Eurocode 3: Design of steel structures - Part 1-12: Additional rules for the extension of EN 1993 up to steel grades S700, 2007.

[19] ASTM International, ASTM E8/E8M-16a: Standard test methods for tension testing of metallic materials, 2016. https://doi.org/10.1520/E0008_E0008M-16A.

[20] F.W. Schutz Jr, N. Newmark, The efficiency of riveted structural joints, 1952.

[21] W.H. Munse, E. Chesson, Riveted and bolted joints: net section design, Journal of the Structural Division. 89(1). (1963). 107-126.

[22] J.W. Fisher, On the behavior of fasteners and plates with holes, 1964.

[23] ABAQUS Analysis User's Manual (Version 6.14), ABAQUS Standard, 2014.

[24] European Committee for Standardization (CEN), BS EN 1993-1-8: Eurocode 3: Design of steel structures - Part 1-8: Design of joints, 2005.

[25] P.W. Bridgman, Studies in large plastic flow and fracture, McGraw-Hill New York, 1952.

[26] L.-J. Jia, H. Kuwamura, Ductile fracture simulation of structural steels under monotonic tension, Journal of Structural Engineering. 140(5). (2014). 04013115. https://doi.org/10.1061/(ASCE)ST.1943-541X.0000944.

[27] X.-P. Pang, Y. Hu, S.-L. Tang, Z. Xiang, G. Wu, T. Xu, X.-Q. Wang, Physical properties of high-strength bolt materials at elevated temperatures, Results in Physics. 13. (2019). 102156. https://doi.org/10.1016/j.rinp.2019.102156.

[28] Y. Bai, Effect of loading history on necking and fracture, PhD. Massachusetts Institute of Technology, Cambridge, USA. (2007).

[29] G.R. Johnson, W.H. Cook, Fracture characteristics of three metals subjected to various strains, strain rates, temperatures and pressures, Engineering fracture mechanics. 21(1). (1985). 31-48.

[30] T. Wierzbicki, Y. Bao, Y.-W. Lee, Y. Bai, Calibration and evaluation of seven fracture models, International Journal of Mechanical Sciences. 47(4). (2005). 719-743. https://doi.org/10.1016/j.ijmecsci.2005.03.003.

[31] D. Dassault Systèmes, Abaqus analysis user’s manual, Vol. 3: Materials, Version 6.14, 2014.

[32] J.R. Rice, D.M. Tracey, On the ductile enlargement of voids in triaxial stress fields∗, Journal of the Mechanics and Physics of Solids. 17(3). (1969). 201-217.

[33] K.K. Adewole, L.H. Teh, Predicting steel tensile responses and fracture using the phenomenological ductile shear fracture model, Journal of Materials in Civil Engineering. 29(12). (2017). 06017019. https://doi.org/10.1061/(ASCE)MT.1943-5533.0002094.

[34] H.K. Farahani, M. Ketabchi, S. Zangeneh, Determination of Johnson–Cook plasticity model parameters for Inconel718, Journal of Materials Engineering and Performance. 26(11). (2017). 5284-5293. https://doi.org/10.1007/s11665-017-2990-2.

[35] E. Corona, G.E. Orient, An evaluation of the Johnson-Cook model to simulate puncture of 7075 aluminum plates, 2014. https://doi.org/10.2172/1204105.

[36] A. Nádai, Theory of flow and fracture of solids, Vol. 1, New Yorkr, 1950.

[37] E.J. Hearn, Mechanics of materials 1: An introduction to the mechanics of elastic and plastic deformation of solids and structural materials, 3rd ed., Elsevier, Englandr, 1997. https://doi.org/10.1016/B978-0-7506-3265-2.X5000-2.

[38] H.H. Snijder, D. Ungermann, J.W.B. Star, G. Sedlacek, F. S.K. Bijlaard, A. Hernmert-Halswick, Evaluation of test results on bolted connctions in order to obtain strength functions and suitable model factor. Part B: Evaluations, Background documentation to Eurocode 3, TNO, Brussels. 1988.

[39] S. G., F. M., K. B., T. D., H. S., M. C., H. W., S. N., D. W., L. P., M. S., B. J., R. J., P. R., B. F., G. Michel, P.V. Artur, D. Silvia, Commentary and worked examples to EN 1993-1-10 "Material toughness and through thickness properties" and other toughness oriented rules in EN 1993, OPOCE, Italy. 2008.

[40] European Committee for Standardization (CEN), BS EN 1990: 2002+ A1: 2005: Eurocode–Basis of structural design, London. 2005.

[41] A. Bond, A. Harris, Decoding Eurocode 7, Taylor and Francis, Londonr, 2008.

[42] M. Byfield, D. Nethercot, Safety variations in steel designed using Eurocode 3, JCSS Workshop on Reliability Based Code Calibration, Zurich: ETH Zurich, 2002.

[43] J. Wang, S. Afshan, M. Gkantou, M. Theofanous, C. Baniotopoulos, L. Gardner, Flexural behaviour of hot-finished high strength steel square and rectangular hollow sections, Journal of Constructional Steel Research. 121. (2016). 97-109. https://doi.org/10.1016/j.jcsr.2016.01.017.

[44] H.H. Snijder, D. Ungermann, J.W.B. Star, G. Sedlacek, F. S.K. Bijlaard, A. Hernmert-Halswick, Evaluation of test results on bolted connctions in order to obtain strength functions and suitable model factor. Part A: Results, Background documentation to Eurocode 3, TNO, Brussels. 1988.

[45] B. Johansson, R. Maquoi, G. Sedlacek, New design rules for plated structures in Eurocode 3, Journal of Constructional Steel Research. 57(3). (2001). 279-311. https://doi.org/10.1016/S0143-974X(00)00020-1.

[46] F. Bijlaard, G. Sedlacek, J. Stark, Procedure for the determination of design resistance from tests. Background report to Eurocode 3" Common unified rules for Steelstructures", 1987.

[47] P. Može, Statistical evaluation of bearing resistance and related strength functions for bolted connections, Journal of Constructional Steel Research. 171. (2020). 106128. https://doi.org/10.1016/j.jcsr.2020.106128.

[48] J. Kouhi, M. Kortesmaa, Strength tests on bolted connections using high-strength steels (HSS Steels) as a base material, Rakenteiden mekaniikka. 25(3). (1992). 41-53.

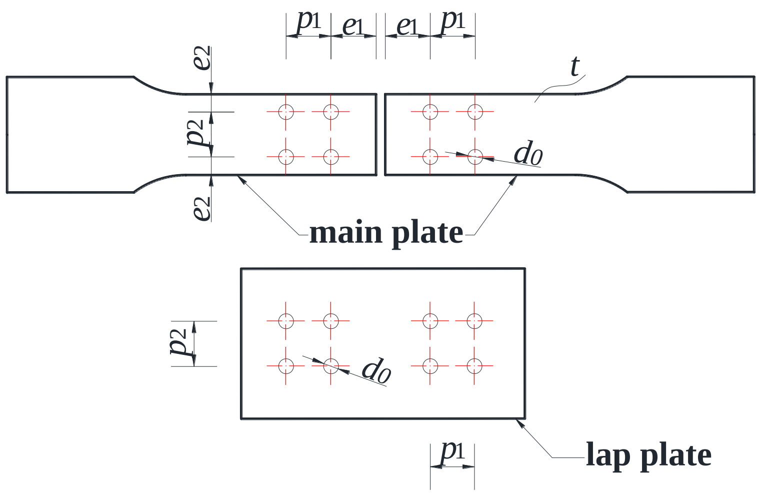

Fig. 1. Geometric configuration of specimens

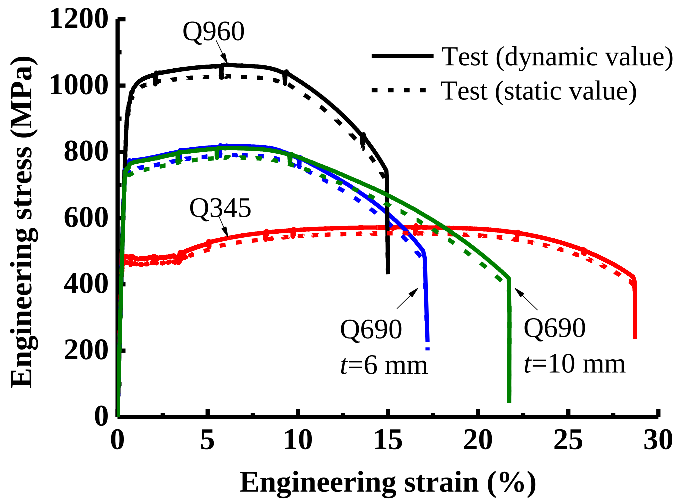

Fig. 2. Typical stress-strain curves of MS and HSS materials

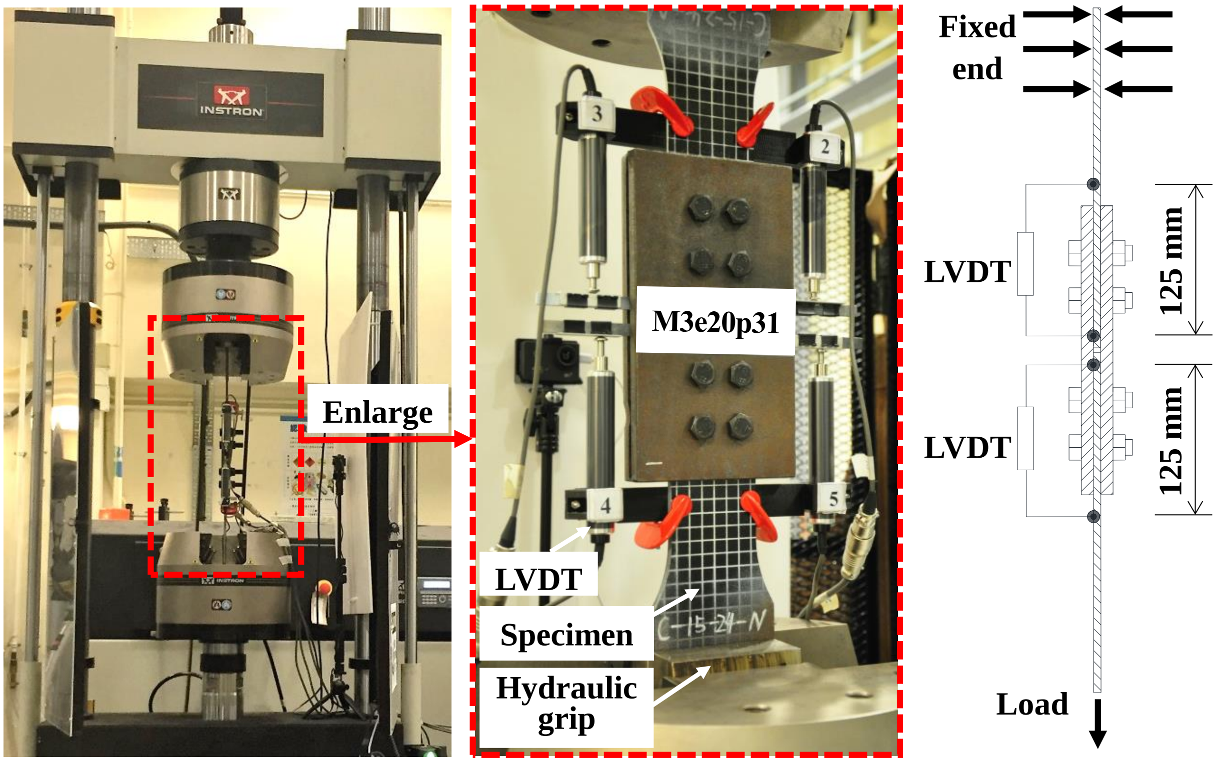

Fig. 3. Test setup

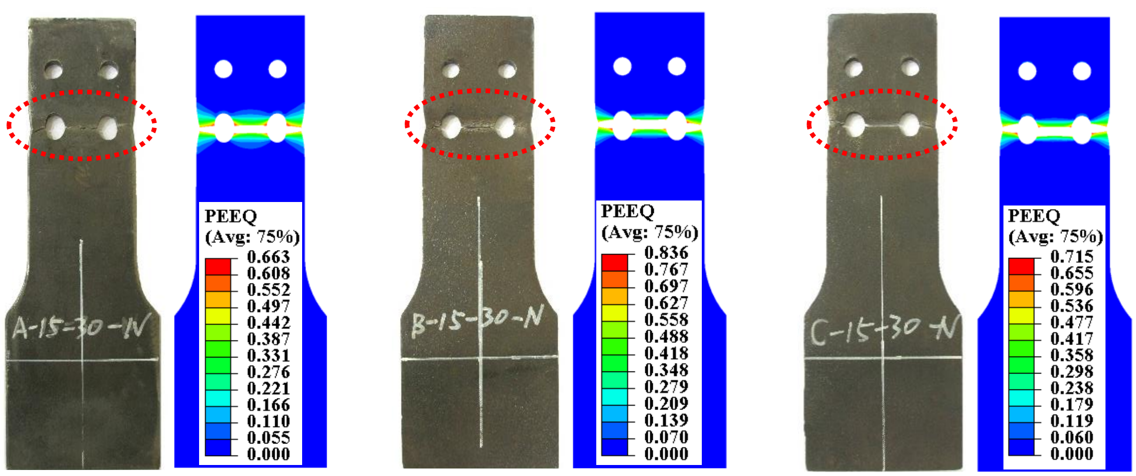

(a) Specimen M1e20p39 (b) Specimen M2e20p39 (c) Specimen M3e20p39

Fig. 4. Typical failure mode of specimens

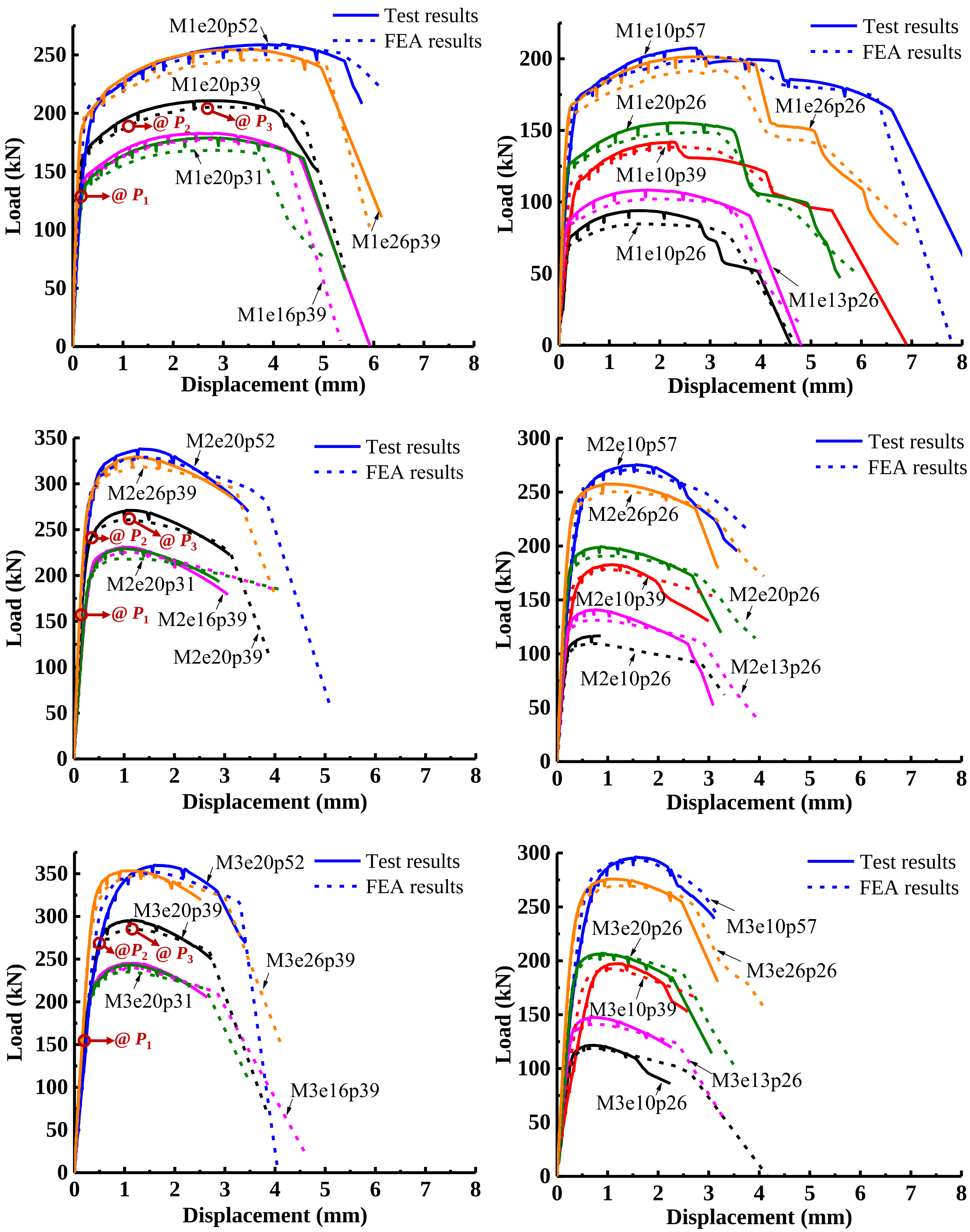

Fig. 5. Load-displacement curves of specimens

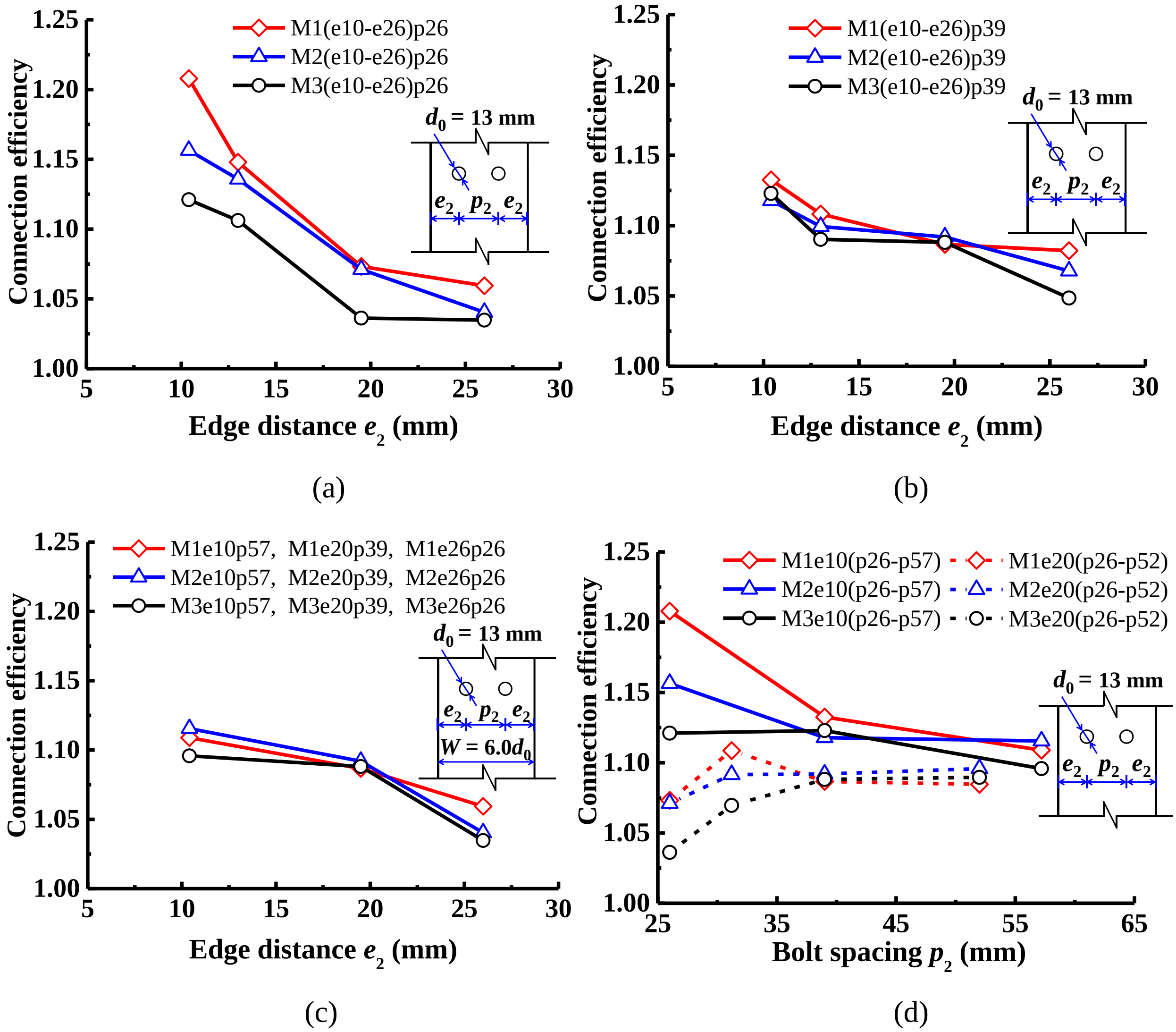

Fig. 6. Effect of edge distance and bolt spacing on the connection efficiency

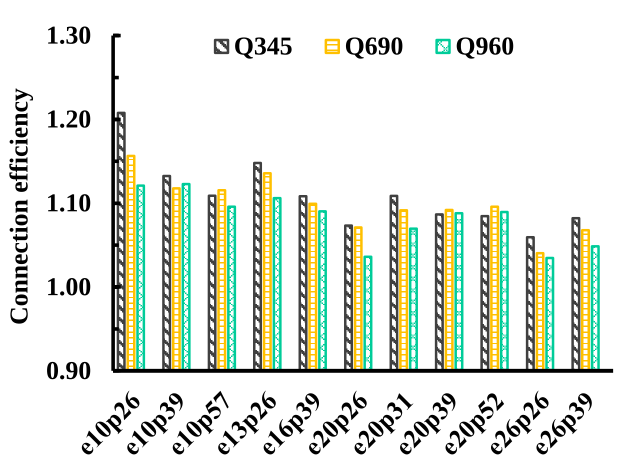

(a) Effect on connection efficiency

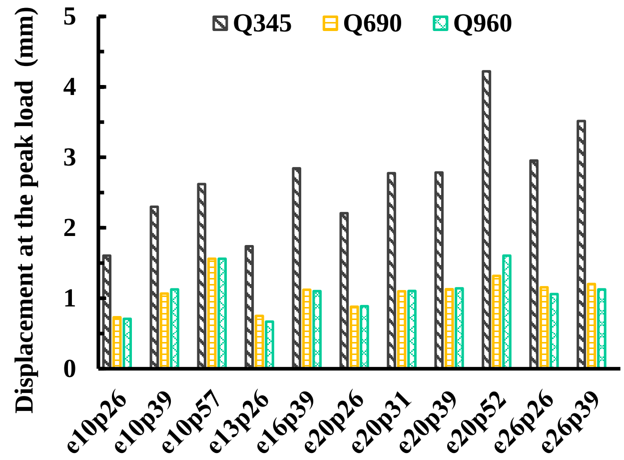

(b) Effect on deformation

Fig. 7. Effect of steel grade on the structural behaviour

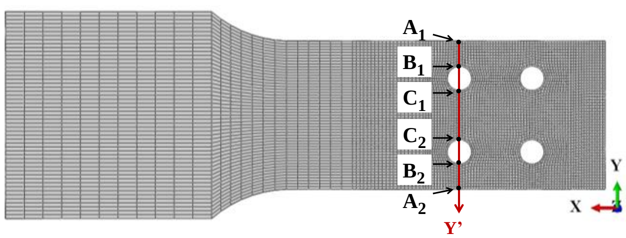

(a) Main plate

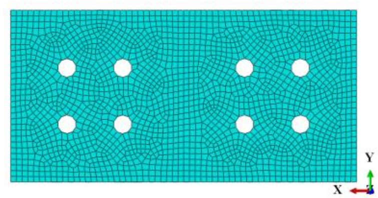

(b) Lap plate

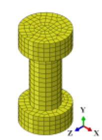

(c) Bolt

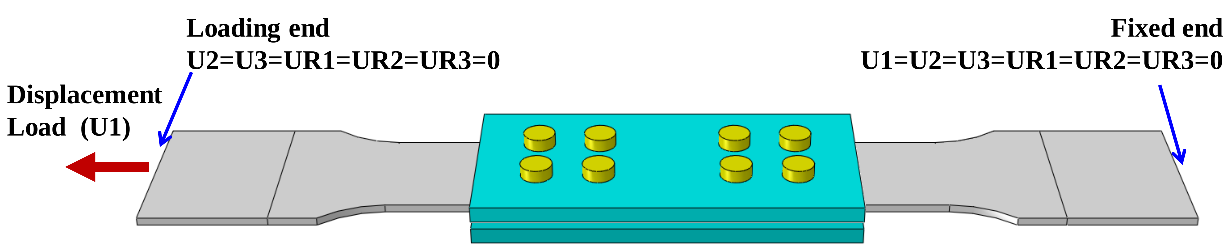

(d) Boundary conditions

Fig. 8. Typical FE model (Specimen M3e20p39)

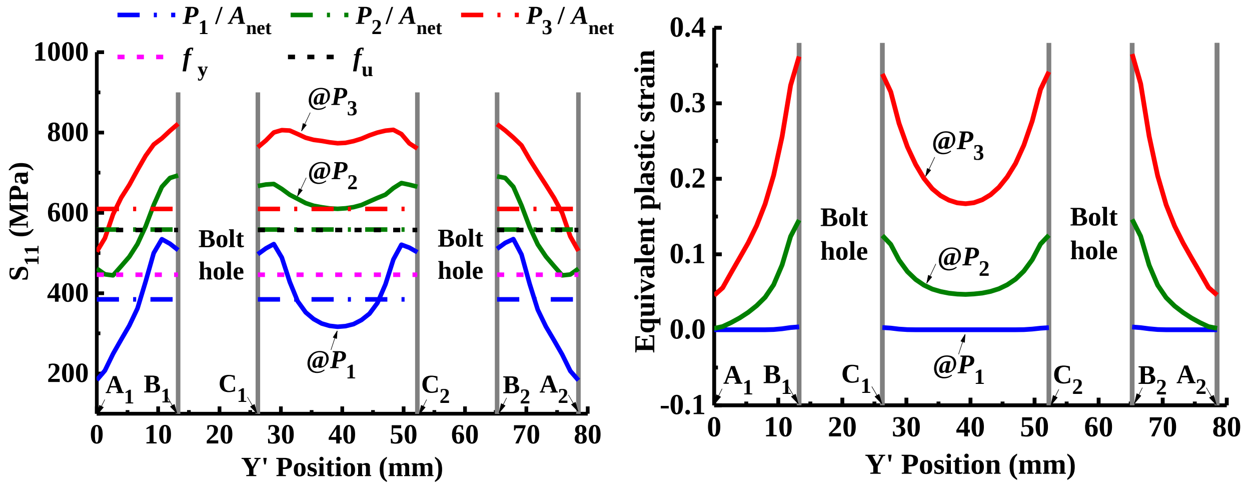

(a) Specimen M1e20p39

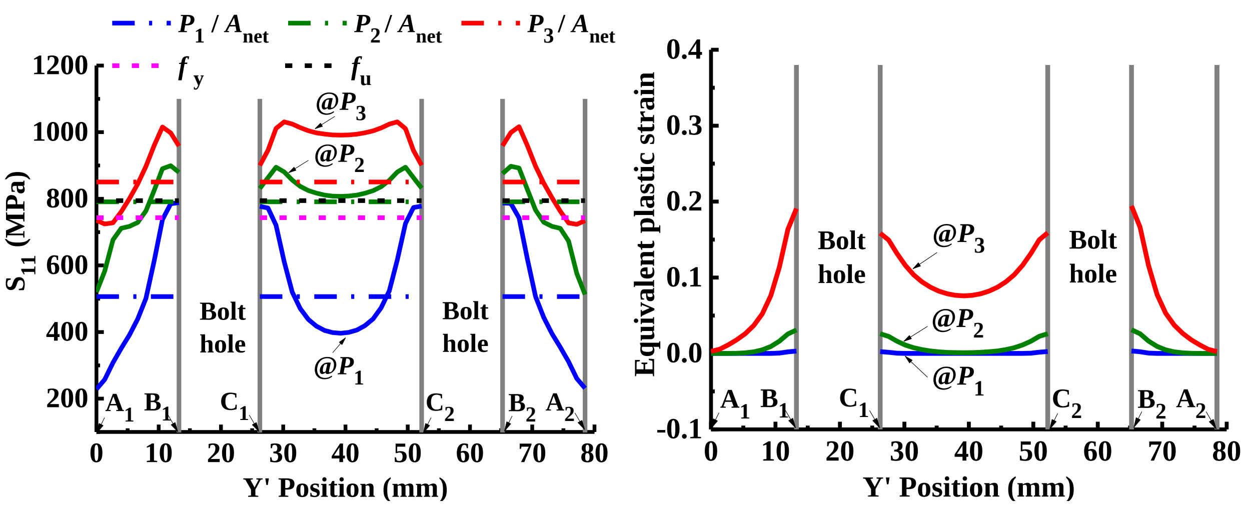

(b) Specimen M2e20p39

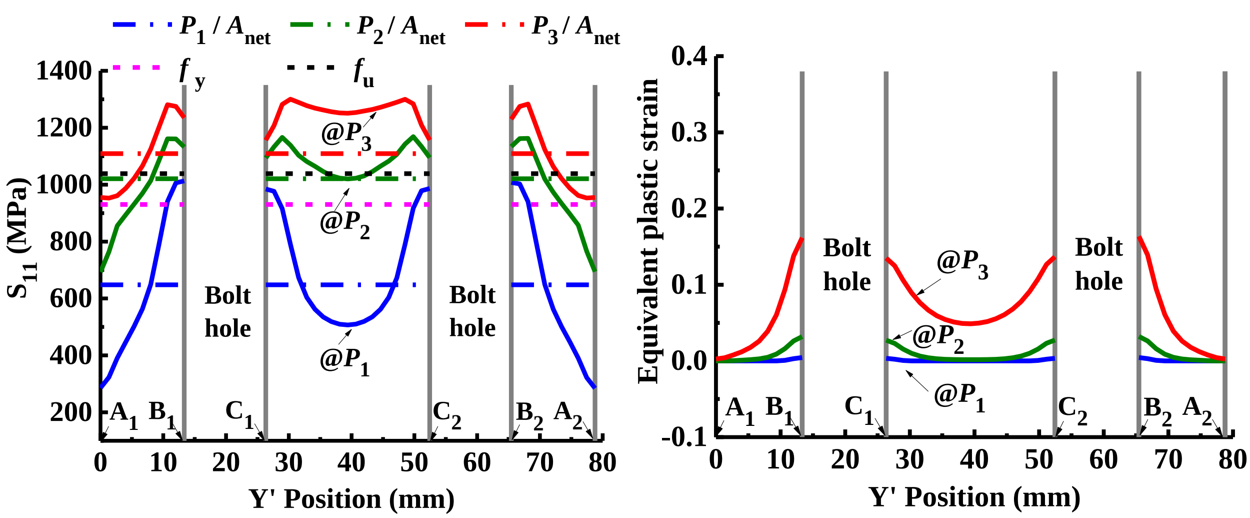

(c) Specimen M3e20p39

Fig. 9. Distribution of stress S_{11} and PEEQ across the critical net section

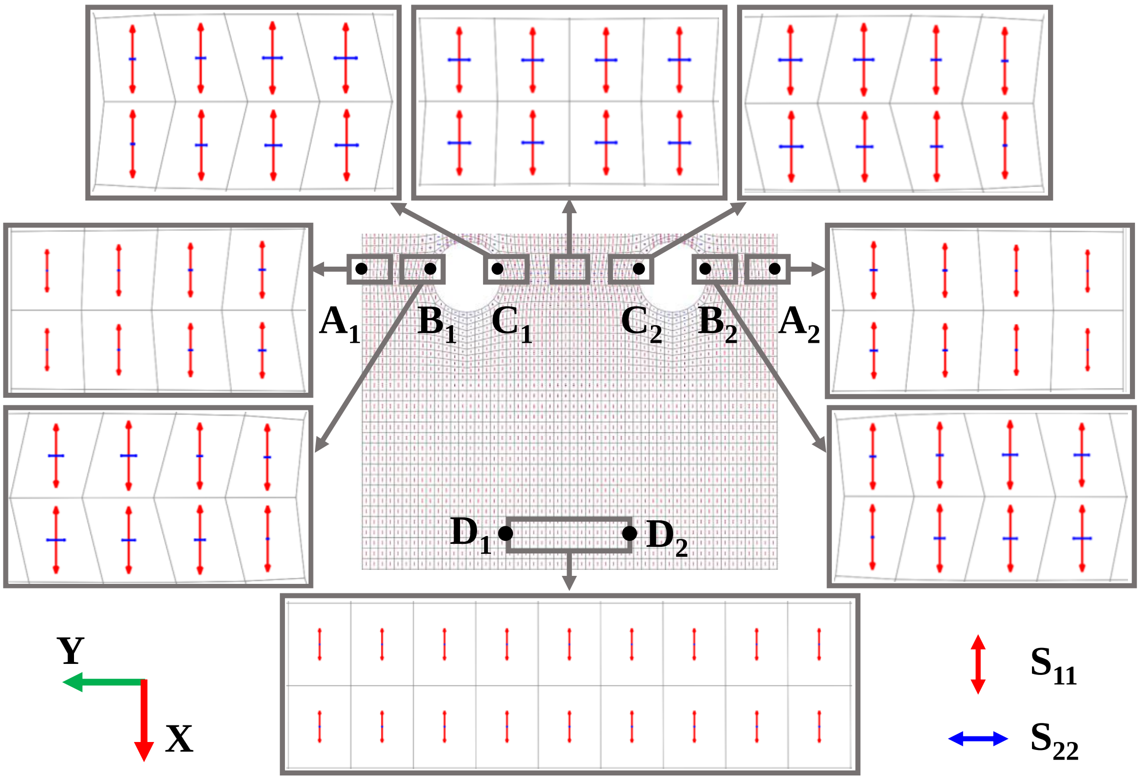

Fig. 10. Net section under biaxial stress at loading stage $0.9P_{\mathrm{u,FEM}}$ (Specimen M3e20p39)

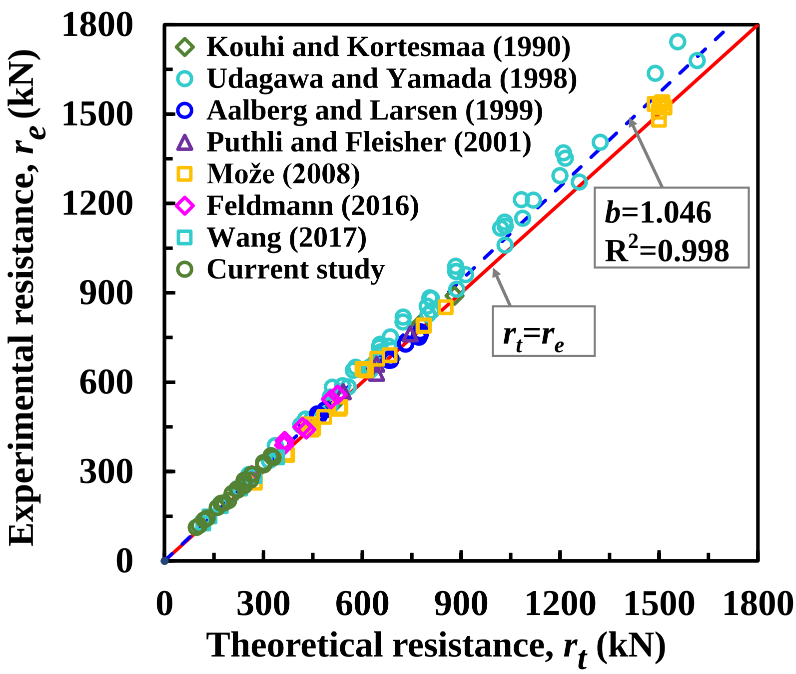

Fig. 11. Statistic evaluation of design model $A_{\mathrm{net}}f_{\mathrm{u}}$ (Set 2 data)

Table 1 Measured dimensions of specimens, test results and FE predictions

No.	Specimen	W (mm)	t (mm)	e_2 (mm)	p_2 (mm)	d_0 (mm)	A_{net} (mm^2)	P_{us} (kN)	$P_{u,test}$ (kN)	$P_{u,test}/P_{us}$	$P_{u,test}/P_{u,FEM}$
1	M1e10p26	47.3	6.3	10.2	26.9	13.1	133.2	74.2	89.7	1.21	1.05
2	M1e10p39	60.1	6.4	10.2	39.8	13.1	217.5	121.2	137.3	1.13	0.99
3	M1e10p57	78.2	6.3	10.2	57.7	13.1	325.7	181.5	201.3	1.11	1.00
4	M1e13p26	52.3	6.3	13.0	26.2	13.3	162.4	90.5	103.9	1.15	1.02
5	M1e16p39	70.6	6.4	15.7	39.2	13.0	285.7	159.2	176.5	1.11	0.99
6	M1e20p26	65.4	6.4	19.9	25.5	13.1	250.1	139.4	149.6	1.07	1.01
7	M1e20p31	70.4	6.3	19.6	31.1	13.1	279.0	155.5	172.4	1.11	1.02
8	M1e20p39	78.5	6.4	19.8	39.0	13.0	336.8	187.7	204.0	1.09	0.99
9	M1e20p52	91.5	6.3	19.7	52.1	13.1	414.3	230.9	250.5	1.08	0.98
10	M1e26p26	78.4	6.3	26.1	26.1	13.1	330.4	184.2	195.1	1.06	1.02
11	M1e26p39	91.5	6.3	26.2	39.0	13.1	409.7	228.4	247.1	1.08	1.01
									Mean	1.11	1.01
									CoV	3.8%	2.0%
12	M2e10p26	47.0	5.8	10.1	26.9	13.1	121.5	96.5	111.6	1.16	1.02
13	M2e10p39	60.5	5.8	10.3	39.8	13.0	201.4	160.0	178.8	1.12	1.00
14	M2e10p57	78.1	5.9	10.2	57.8	13.1	304.2	241.7	269.6	1.12	0.99
15	M2e13p26	52.2	5.8	13.1	26.1	13.1	151.8	120.6	137.0	1.14	1.04
16	M2e16p39	70.5	5.8	15.7	39.1	13.0	258.6	205.4	225.8	1.10	1.00
17	M2e20p26	65.4	5.8	19.9	25.5	13.1	228.7	181.7	194.6	1.07	1.02
18	M2e20p31	70.4	5.8	19.6	31.2	13.1	258.4	205.3	224.1	1.09	1.03
19	M2e20p39	78.4	5.8	19.7	39.0	13.1	305.0	242.3	264.6	1.09	1.01
20	M2e20p52	91.4	5.8	19.6	52.2	13.1	378.4	300.6	329.5	1.10	1.00
21	M2e26p26	78.0	5.9	25.9	26.1	13.1	304.9	242.2	252.0	1.04	1.01
22	M2e26p39	91.0	5.8	26.0	39.0	13.1	379.1	301.2	321.6	1.07	1.01
23	M3e10p26	47.0	4.9	10.0	27.0	13.1	101.6	105.5	118.3	1.12	0.99
24	M3e10p39	60.0	4.9	10.1	39.9	13.1	165.4	171.8	192.9	1.12	1.00
25	M3e10p57	78.3	4.9	10.2	57.9	13.1	254.7	264.5	289.9	1.10	0.99
26	M3e13p26	52.0	4.8	13.0	26.0	13.1	124.6	129.4	143.2	1.11	1.01
27	M3e16p39	70.2	4.8	15.5	39.3	13.1	211.7	219.9	239.7	1.09	1.00
28	M3e20p26	65.3	4.8	19.9	25.5	13.1	187.7	194.9	202.0	1.04	0.98
29	M3e20p31	70.4	4.8	19.5	31.3	13.1	213.8	222.0	237.5	1.07	1.01
30	M3e20p39	78.8	4.9	19.8	39.1	13.1	256.6	266.4	289.9	1.09	1.02
31	M3e20p52	90.8	4.8	19.3	52.2	13.1	311.6	323.6	352.6	1.09	1.00
32	M3e26p26	78.4	4.8	26.1	26.2	13.1	251.7	261.4	270.5	1.03	1.00
33	M3e26p39	91.0	4.9	26.0	39.0	13.1	317.2	329.5	345.5	1.05	0.99
									Mean	1.09	1.01
									CoV	3.0%	1.4%

Note: The nominal thickness of the main plate is 6.0 mm, 6.0 mm and 5.0 mm for Q345, Q690 and Q960 steel plates, respectively. The nominal diameter of each bolt and bolt hole is 12.0 mm and 13.0 mm, respectively.

Table 2 Mean value of the measured material properties

Material	Elastic modulus, E (GPa)	Static yield strength, f_y (MPa)	Static tensile strength, f_u (MPa)	Ultimate strain, ε_u (%)	Elongation at fracture, Δ (%)	f_u/f_y
Q345 (t=6 mm)	212.2	446.1	557.4	16.81	29.47	1.25
Q690 (t=6 mm)	204.8	743.2*	794.5	6.14	17.37	1.07
Q690 (t=10 mm)	206.1	742.7*	791.0	6.91	22.30	1.07
Q960 (t=5 mm)	203.7	930.2*	1038.5	6.10	15.67	1.10

*Note: * -- 0.2% proof stress*

Table 3 Results of statistical analyses of design net section resistance

Design model	**Data set**	**Number of tests**	k_n	k_d	b	V_δ	V_r	k_c	γ_M	$\gamma_M{}^*$
$A_{net}f_u$	1	22	1.76	3.61	1.081	0.030	0.080	0.948	1.124	1.066
	2	137	1.64	3.04	1.046	0.045	0.087	0.989	1.129	1.118
	3	69	1.68	3.24	1.072	0.036	0.083	0.960	1.126	1.080
	4	68	1.68	3.24	1.012	0.049	0.089	1.028	1.138	1.170
$0.9A_{net}f_u$	1	22	1.76	3.61	1.201	0.030	0.080	0.853	1.124	0.960
	2	137	1.64	3.04	1.163	0.045	0.087	0.891	1.129	1.006
	3	69	1.68	3.24	1.192	0.036	0.083	0.864	1.126	0.972
	4	68	1.68	3.24	1.124	0.049	0.089	0.926	1.138	1.053

Note: set 1 - the new HSS connection data from this study; set 2 - all test data from current study and existing literature; set 3 and 4 - test data of specimens with a yield strength lower and greater than 700 MPa, respectively, from set 2.

Table 4 Test results collected from existing literature

Reference	**No. of tests**	N_b	W **(mm)**	t **(mm)**	d_0 **(mm)**	f_y **(MPa)**	f_u **(MPa)**
Kouhi and Kortesmaa (1990) [48]	5	Nil	Nil	Nil	Nil	622	733
Udagawa and Yamada (1998) [14]	49	2-3	110-242	12.0	18	460-674	596-800
Aalberg And Larsen (1999) [9]	18	1	110	10.0	22-32	472-820	556-873
Puthli and Fleisher (2001) [11]	4	2	108-135	17.5	30	524	645
Može (2008) [7]	25	1-2	60-198	10.0	24-30	796-847	844-885
Feldmann et al. (2016) [12]	8	1	60-90	8.0	30	1060	1161
Wang et al. (2017) [8]	6	1	41-58	10.0	26	677-1022	757-1064
Current study	22	2	47-92	5.0-6.0	13	743-930	794-1039
Total	**137**	**1-3**	**41-242**	**5.0-17.5**	**13-32**	**460-1060**	**556-1161**

Note: For specimens in Kouhi and Kortesmaa (1990), the values of net section area, ultimate load and design resistance were extracted from Može (2008); For specimens in Feldmann et al. (2016), the corresponding values were extracted from the Figure of comparison between experimental and theoretical resistance in the literature.

Conflict of Interest

There is no financial/personal interest or belief that could affect our objectivity. There are no potential conflicts of interest either.

CRediT authorship contribution statement

Xue-Mei Lin: Writing - original draft, Methodology, Software, Validation, Formal analysis, Investigation, Visualization.

Michael C.H. Yam: Conceptualization, Resources, Writing - review & editing, Supervision, Project administration, Funding acquisition.

Kwok-Fai Chung: Resources, Writing - review & editing

Angus C.C. Lam: Writing - review & editing